

Application of Scanning Electron-Acoustic Microscopy to Biological Materials

**Chun-ming Gao,¹ Shu-yi Zhang,^{1,2} Peng-cheng Miao,¹
Zhong-ning Zhang,¹ and Ping Li³**

Received July 1, 2003

The imaging methods and results for biological materials by scanning electron acoustic microscopy (SEAM) have been introduced in this paper. The images of the amplitude and phase of a plant leaf by SEAM show that the amplitude image involves more surface features but the phase image displays more subsurface structures. The laminated imaging experiments, which use the x - and y -components of SEAM signals with different reference phases, show the subsurface structures in different depths of biological materials, such as, plant leaves, biological tissues, etc. Using a photothermal technique, the thermal diffusion lengths of the samples of biological materials can be evaluated, by which the depths of the subsurface structures in the laminated images can be estimated. In addition, the damage areas of the leaf and muscles are also imaged by SEAM. For comparison, the second electron images of the same areas of the samples studied by SEAM are also obtained. The images show that SEAM is sensitive to micro-structures of surface, and also subsurface, structures of biological materials.

KEY WORDS: biological materials; electron-acoustic microscopy; laminated imaging; subsurface structure.

1. INTRODUCTION

Scanning electron-acoustic microscopy (SEAM) has been widely used for imaging and analyzing of many kinds of non-biological materials [1–5],

¹ Lab of Modern Acoustics, Institute of Acoustics, Nanjing University, Nanjing 210093, P. R. China.

² To whom correspondence should be addressed. E-mail: paslab@nju.edu.cn

³ The First Hospital of Nanjing, Nanjing University of Medicine, Nanjing 210006, P. R. China.

especially for biomedical materials [3, 5]. Based on the principle of laminated imaging of photoacoustic thermal wave microscopy [6], a laminated imaging system of SEAM has been established [7]. The spacial resolution and the signal-to-noise ratio are improved by enhancing the intensity and the modularity of the electron beam. As we have known, the amplitude images show mainly surface topographs and the phase images show the subsurface structures. The images obtained at different modulation frequencies involve the structures in different depth ranges of the samples. On the other hand, the vector imaging, i.e., the imaging by x or y component of the SEAM signals, the images with different reference phases show the structures at different depths of the samples. Using frequency and phase adjusting of SEAM, the laminated imaging experiments have been successfully performed for several materials and structures, such as integrated circuits with submicron structures, ferroelectric domains of PZT, crystal shapes of metals, depth distributions of residual stress in aluminum alloys indented by a micro-indenter or induced by a high intensity laser beam, etc., which demonstrate that SEAM system is very sensitive and versatile.

Also, the system is used for analyzing some biological materials, such as, leafs of plants, tissues of liver, heart, muscle of rats, and cornea of human. The micro-structures, such as muscle fibers, blood vessels, voids, and others are shown clearly in SEAM laminated images. In addition, damage experiments of biological tissues have also been done, in which the damaged area impinged by an electron beam or laser beam is very clearly displayed in SEAM images. In order to make comparisons, scanning electron microscopy (SEM) images of the same samples are also obtained. It is shown that the subsurface structures or damaged areas of the samples can scarcely be seen in SEM images.

2. METHODS

The experimental system of SEAM is a modified scanning electron microscope, in which the electron beam is intensity-modulated at a frequency f and focused on the sample. The local periodic heating of the sample surface produces a thermal wave and then an acoustic wave. The solution of the heat diffusion equation shows that the thermal diffusion length μ_1 is expressed as [8]

$$\mu_1 = \sqrt{\lambda / (\pi f \rho C)} \quad (1)$$

where λ , ρ , and C are the thermal conductivity, density, and specific heat of the sample, respectively. But the thermal wave is so highly damped

that it typically propagates no more than a thermal diffusion length. The surface and subsurface features within μ_t of the sample may serve as scatterers as the thermal wave propagates; thus, an acoustic signal will be generated as a result of thermal-to-acoustic mode conversion. A piezoelectric transducer (PZT) in tight contact with the bottom of the sample converts the acoustic signals into electrical signals. In order to amplify the signals and suppress the noise, a preamplifier and then a lock-in amplifier are used, and then the output of a PZT is amplified and mixed with a reference signal by the lock-in amplifier. The final imaging signal \bar{V} is [6]:

$$\bar{V} = \int_0^{x_m} |V(x')| \cos[\psi x' - \psi_0] dx' \quad (2)$$

where x_m is the maximum penetration depth of the thermal wave, $V(x')$ and $\psi(x')$ are the output voltage and the phase lag caused by the thermal source at point x' , and ψ_0 is the phase shift of the reference signal of a lock-in amplifier. The output signal \bar{V} reflects the structures of the sample in the thermal-wave penetration range.

It is possible to get different images by varying the frequency to display the properties and structures in different depth ranges because the thermal diffusion length is inversely proportional to the square root of f . On the other hand, the phase of the thermal source $\psi(x')$ is the same as the reference phase ψ_0 and the imaging signal approaches a maximum, i.e., the imaging signal contributed by the structure at x' can be strengthened by the lock-in amplifier. Thus, the laminated imaging can be obtained by changing the reference phase.

In our SEAM, the electron beam can be modulated over the frequency range of 1 kHz to 1 MHz with an accelerated voltage of 20–30 kV. The SEAM signal is detected by PZT disks with different thicknesses, bonded to the bottom of the sample, and fed to a wide-band preamplifier and then a lock-in amplifier with a bandwidth up to 1 MHz. Both the amplitude and phase of the output of the lock-in amplifier can be acquired and processed by a computer. Finally, the amplitude A and phase ψ images of the SEAM signal can be obtained and displayed on the monitor of the computer. Meanwhile, the images corresponding to the x component $A \cos(\psi - \psi_0)$ and y component $A \sin(\psi - \psi_0)$ of the SEAM signal can also be received by the lock-in amplifier and displayed by the monitor. The x -component and y -component images show two different structures at different depths of the sample, in which the detected depth depends on the reference phase ψ_0 . By changing the reference phase,

the laminated images with different depths can be obtained. On the other hand, the SEM image can be obtained in the same area of the sample for comparison.

3. EXPERIMENTAL RESULTS AND DISCUSSIONS

3.1. Preparation and Characteristics of Biological Samples

The samples with a thickness of about 1 mm are prepared as usual as for scanning electron microscopy. For biological materials, the process includes five steps: (1) Cleaning the samples with saline solution; (2) fixing the samples with glutaraldehyde and osmium tetroxide solutions; (3) dehydrating the samples gradually with acetone; (4) evaporating the residual water in the samples with a critical-point dryer; and (5) plating very thin gold film on the surface of the samples.

In order to evaluate the imaging depth (d), the thermal diffusion length μ_t is measured by a photothermal technique; the thermal diffusion length of the biological samples are in the range of 10–20 μm when the modulation frequency is 200 kHz. In addition, because the electron penetration depth d_0 ($d_0 = V^{1.43}/20\rho$, V = acceleration voltage, ρ = density of the sample) is less than ten percent of the thermal diffusion length, so we ignore the influence of the penetration depth on the laminated image depth.

3.2. Amplitude Image and Phase Image of Phoenix Leaf

Figure 1 shows the images of a phoenix leaf: a, the SEM image, b, the SEAM images at the modulation frequency of 184 kHz: (1) amplitude image and (2) phase image. Many netted vein structures and gas holes at



Fig. 1. Images of phoenix leaf: (a) SEM image; (b) SEAM images at $f = 184$ kHz: (1) amplitude image; (2) phase image.

the surface are shown clearly in the SEM image (Fig. 1a). The amplitude image of the SEAM in Fig. 1b (1) is similar to the SEM image, but the microstructures are less clear, which means the amplitude imaging of the SEAM is with lower resolution than the SEM imaging for the leaf due to the influence of some subsurface structures. The phase image in Fig. 1b (2) just shows a few structures, which means the phase image is not sensitive to the surface structures, but may involve mainly information on the subsurface.

3.3. Laminated Imaging of Biological Tissues

At first, the SEM images of the plant leaf and medical tissues are obtained for comparison. Then the imaging experiments of x components of SEAM signals are carried out with different reference phases. In these experiments, some laminated images of the subsurface structures at different depths are displayed in the SEAM images, which are not shown in the SEM images.

3.3.1. Laminated Imaging of Loquat Leaf

An SEM image of a loquat leaf is shown in Fig. 2a, and then five SEAM images of the same area shown in Fig. 2b (1)–(5) are obtained

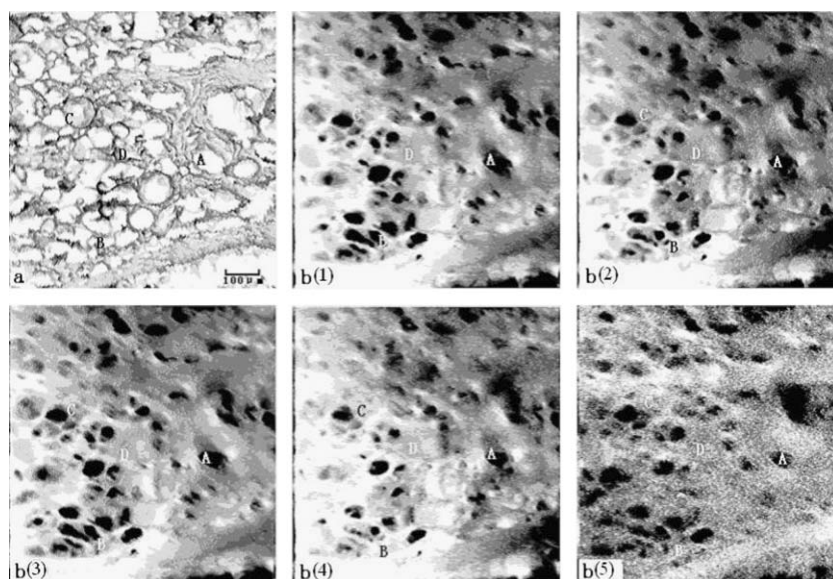


Fig. 2. Images of leaf tissues: (a) SEM image; (b) SEAM images at $f = 200$ kHz and $\mu_t \approx 10$ μm : (1) $\theta = 20^\circ$, $d \approx 0.9$ μm ; (2) $\theta = 60^\circ$, $d \approx 3.3$ μm ; (3) $\theta = 100^\circ$, $d \approx 5.6$ μm ; (4) $\theta = 140^\circ$, $d \approx 7.8$ μm ; (5) $\theta = 180^\circ$, $d \approx 10$ μm .

at a modulation frequency of 200 kHz and the reference phase changes from 20° to 180° . The nervations, fibers, and holes are shown in the SEM image, but only the holes are shown clearly in the SEAM laminated images with different reference phases. In addition, in comparing the images from Fig. 2b (1)–(5), the size of hole A becomes smaller as the phase increases, i.e., as the depth increases; for positions B and C, also, some small structures change gradually with variations in the depth.

In general, by using SEAM in research on plant tissues, more information on subsurface features can be displayed without destructive incision.

3.3.2. Laminated Imaging of Biomedical Tissues

3.3.2.1. Laminated Imaging of Cornea Tissue of Human An SEM image and five SEAM images of a human cornea are shown in Fig. 3. In the SEM image (Fig. 3a) many micro-structures are shown at the surface of the cornea, which are not displayed clearly in the SEAM images. However, some variations of the subsurface structures with depth are shown in Fig. 3b (1)–(5), such as a funnel-like structure in position A as shown clearly in all images of Fig. 3b. Comparing the five SEAM images, the size of the funnel ventage increases from Fig. 3b (1)–(4) and then almost

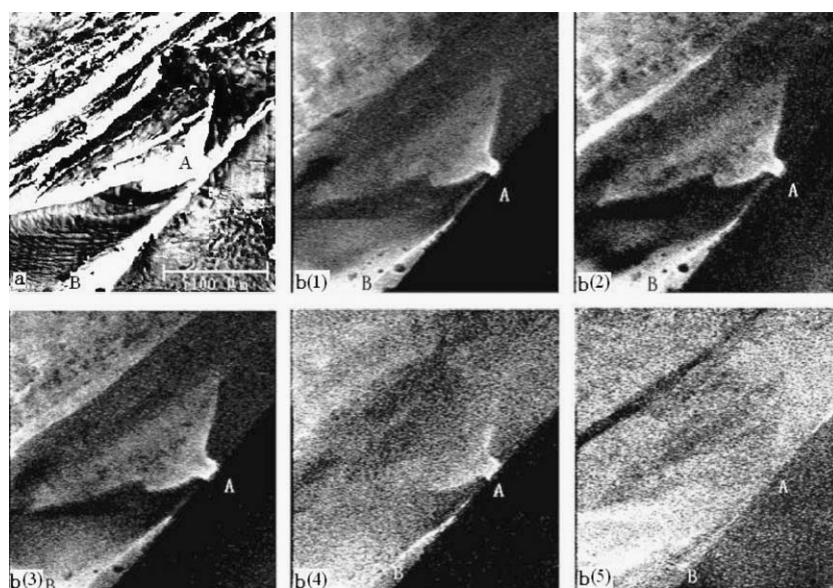


Fig. 3. Images of a human cornea tissues: (a) SEM image; (b) SEAM images at $f = 205$ kHz and $\mu_t \approx 15 \mu\text{m}$: (1) $\theta = 10^\circ$, $d \approx 0.84 \mu\text{m}$; (2) $\theta = 25^\circ$, $d \approx 2.09 \mu\text{m}$; (3) $\theta = 55^\circ$, $d \approx 4.59 \mu\text{m}$; (4) $\theta = 145^\circ$, $d \approx 12.1 \mu\text{m}$; (5) $\theta = 175^\circ$, $d \approx 14.6 \mu\text{m}$.

disappears in Fig. 3b (5), which illustrates probably the related structure is almost located in the range of the imaging depth of Fig. 3b (5). By evaluating the thermal diffusion length of the tissue, a depth of the funnel structure of about $15 \mu\text{m}$ is estimated. In addition, for position B, some structures in the subsurface also change gradually from Fig. 3b (1) to (5).

3.3.2.2. Laminated Imaging of Heart Tissue of Rat An SEM image and three SEAM images of envelope tissues of a rat heart are shown in Fig. 4. In the SEM image (Fig. 4a), some netted surface structures are shown clearly. In the SEAM images, the imaging depths become deeper from Fig. 4b (1) to (4). For position A, a fiber-like structure becomes thinner and then break down from Fig. 4b (1) to (4). For positions B, C, and D, the micro-structures in Fig. 4b (1)–(3) also vary gradually from b (1) to b (4).

3.3.2.3. Laminated Imaging of Liver Tissue of Rat An SEM image and three SEAM images of a rat liver are shown in Fig. 5. A fistular structure is cross through the whole tissues from position A to positions B, C, and D. The SEM image (Fig. 5a) shows the shape of the fistulae on the surface, which has different depths in different parts. From Fig. 5b (1)

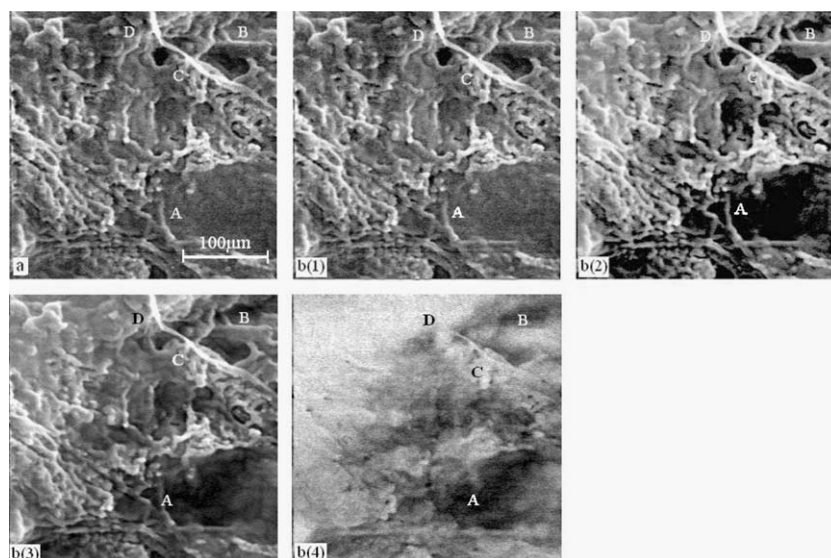


Fig. 4. Images of heart tissues of a rat: (a) SEM image; (b) SEAM images at $f = 200 \text{ kHz}$ and $\mu_t \approx 20 \mu\text{m}$: (1) $\theta = 0^\circ$, $d \approx 0 \mu\text{m}$; (2) $\theta = 45^\circ$, $d \approx 5 \mu\text{m}$; (3) $\theta = 90^\circ$, $d \approx 10 \mu\text{m}$; (4) $\theta = 135^\circ$, $d \approx 15 \mu\text{m}$.

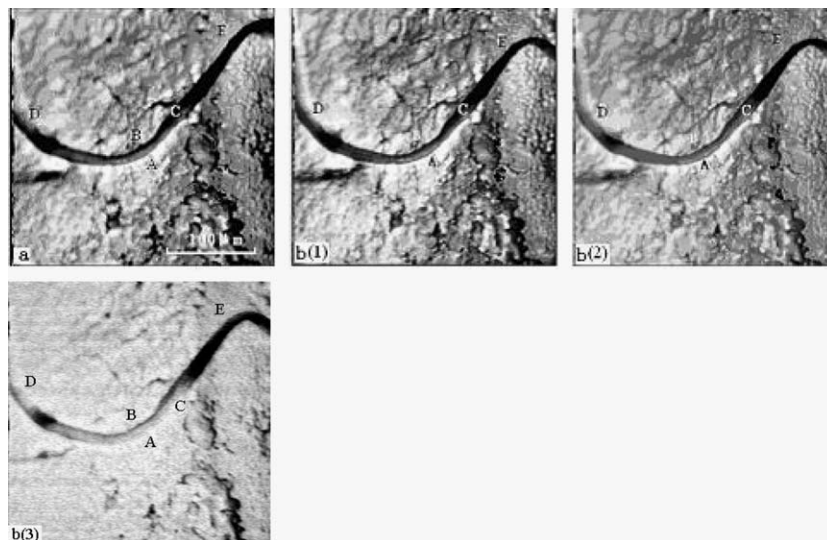


Fig. 5. Images of liver tissues of rat: (a) SEM image; (b) SEAM images at $f = 198$ kHz and $\mu_1 \approx 20$ μm ; (1) $\theta = 0^\circ$, $d \approx 45$ μm ; (3) $\theta = 135^\circ$, $d \approx 15$ μm .

to (3), the imaging depth approaches gradually to the depth of the back-side wall of the fistular structure, which is about 20 μm . For position C, some small micro-structures also change from Fig. 5b (1) to (3).

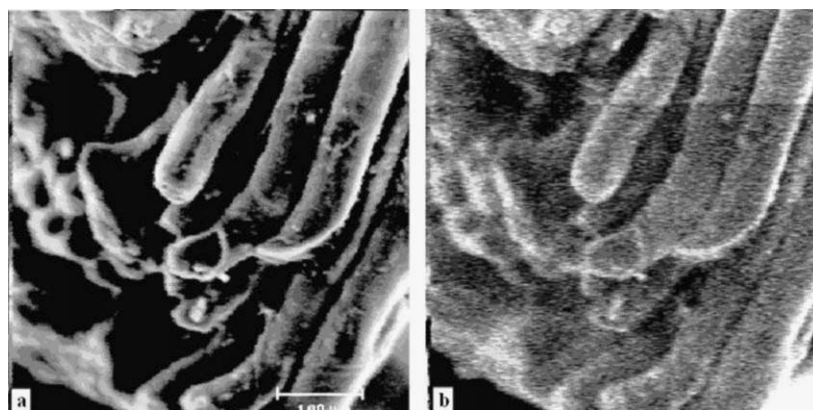


Fig. 6. Images of muscle tissues of rat irradiated and damaged by a high energy electron beam: (a) SEM image; (b) SEAM image of amplitude at $f = 197$ kHz.

3.4. Damage of Biological Tissue

As we know biological tissues are always damaged by a laser beam (such as human skin or retina), or an electron beam (samples in SEM). In this section, some damaged images are discussed.

(1) An electron beam with 30 kV of SEM is used to irradiate a muscle tissue of rat for half an hour, then images of the damaged area by SEM and SEAM are shown in Fig. 6. Some muscle fibers are shown in

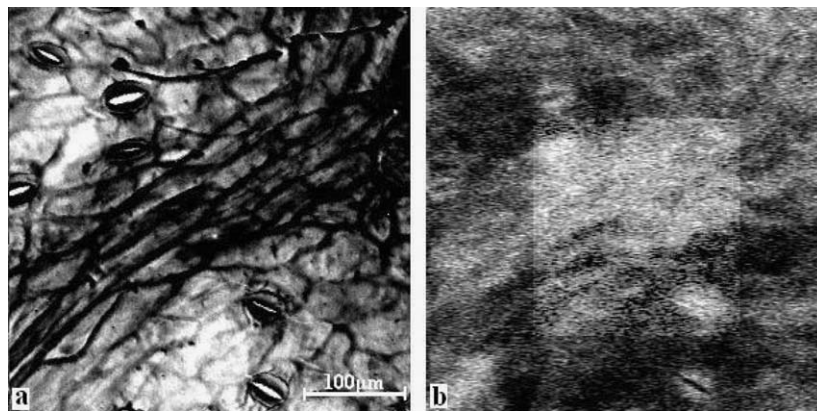


Fig. 7. Images of a poplar leaf irradiated and damaged by a high energy electron beam: (a) SEM image; (b) SEAM image of amplitude at $f = 202$ kHz.

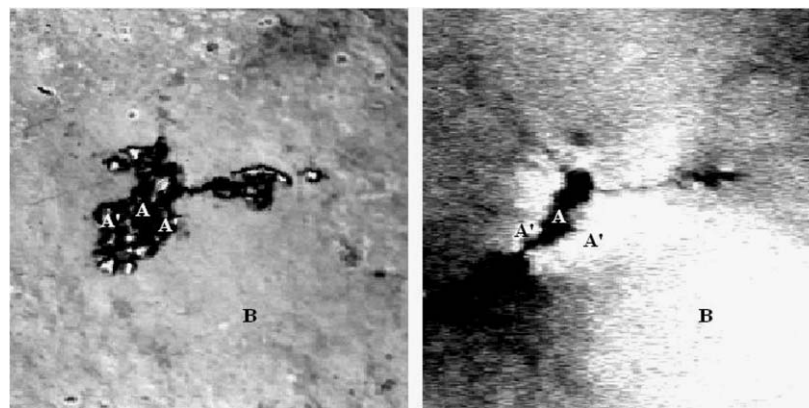


Fig. 8. Images of a poplar leaf irradiated and damaged by a laser beam irradiation: (a) SEM image; (b) SEAM image of amplitude at $f = 202$ kHz.

both Fig. 6a, b, but the damaged area as a square block is shown in the SEAM image (Fig. 6b) only.

Another damage experiment is carried out for a poplar leaf with the same method. The SEM image (Fig. 7a) shows clearly the gas holes, nervations, and cells on the surface, but the SEAM image also shows a square block of the damaged area (Fig. 7b).

(2) A laser beam is used to irradiate a loquat leaf, and the laser is so strong that hole A is formed, which can be seen in Fig. 8; meanwhile, the neighbor area A' of the hole is withered. In the SEM picture (Fig. 8a), it is difficult to distinguish the different A and A' areas, but they are easy to distinguish in the SEAM picture (Fig. 8b). For area B, which is slightly damaged, the different structures compared with other areas are shown in Fig. 8b, but not in Fig. 8a.

4. CONCLUSIONS

From the SEM and SEAM imaging results and discussions for biological tissues, several conclusions can be drawn.

- (1) SEAM established on the basis of SEM can be used to analyze the subsurface structures of biological tissues.
- (2) Due to the thermal wave excited by an electron beam having a limited penetration length, it is possible to get imaging of the subsurface structures of the samples. Since the diffusion length is inversely proportional to the square root of the modulation frequency, the structure images at different depths can be obtained by changing the modulation frequency of the electron beam.
- (3) The signal of SEAM is an integration of the signals contributed by the thermal wave sources distributed in the penetration length, the surface resolution of it is lower than that of SEM for some tissues, because of the influence of the subsurface structures.
- (4) Since the signal produced by the thermal source (subsurface structure) at different depths has different phase lags, laminated imaging of biological tissues can be obtained by adjusting the reference phase of the lock-in amplifier.
- (5) As the thermal penetration length of the biological tissues can be evaluated by a photothermal technique, the depth of the laminated imaging can also be estimated.
- (6) Generally, SEAM can provide some special information on the subsurface structures of biological tissues, which cannot be obtained by SEM.

- (7) Imaging depths must be estimated more precisely, and these studies are currently in progress.

ACKNOWLEDGMENT

National Natural Science Foundation of China, No. 10174038, supports this work.

REFERENCES

1. G. S. Cargill, III, *Nature* **286**:691 (1980).
2. E. Brandis and A. Rosencwaig, *Appl Phys. Lett.* **37**:98 (1980).
3. L. J. Balk, M. Domnik, and E. Bohm, *SPIE* **809**:219 (1987).
4. L. X. Liu and L. J. Balk, *J. Mat. Sci.* **33**:4543 (1998).
5. L. J. Balk, *Adv. Electron. Electron Phys.* **71**:1 (1988).
6. S. Y. Zhang and L. Chen, in *Photoacoustic and Thermal Wave Phenomena in Semiconductors*, A. Mandelis, ed. (Elsevier, Amsterdam, 1987), pp. 27–52.
7. Y. Hong, Z. N. Zhang, S. Y. Zhang, Z. Q. Li, and X. J. Shui, *Acoustical Imaging*, Vol. 25, P. N. T. Wells and M. Halliwell, eds. (Kluwer Academic/Plenum Pubs., New York, 2000), p. 273.
8. L. J. Balk, M. Domnik, K. Niklas, and P. Mestres, *Photoacoustic and Photothermal Phenomena II*, *Springer Series in Optical Sciences*, Vol. 62, J. C. Murphy, J. W. Maclachlan-Spider, and B. S. H. Royce, eds. (Springer-Verlag, Berlin, 1990).